GPR183 antagonism reduces macrophage infiltration in influenza and SARS-CoV-2 infection

Cheng Xiang Foo[1,8], Stacey Bartlett[1,8], Keng Yih Chew[2], Minh Dao Ngo[1], Helle Bielefeldt-Ohmann[2,3], Buddhika Jayakody Arachchige[4], Benjamin Matthews[4], Sarah Reed[4], Ran Wang[1], Christian Smith[1], Matthew J. Sweet[3,5], Lucy Burr[6], Kavita Bisht[1], Svetlana Shatunova[1], Jane E. Sinclair[2], Rhys Parry[2], Yuanhao Yang[1], Jean-Pierre Lévesque[1], Alexander Khromykh[2,3], Mette Marie Rosenkilde[7], Kirsty R. Short[2,3] and Katharina Ronacher[1,3]

[1]Mater Research Institute, Translational Research Institute, The University of Queensland, Brisbane, Australia. [2]School of Chemistry and Molecular Biosciences, The University of Queensland, Brisbane, Australia. [3]Australian Infectious Diseases Research Centre, The University of Queensland, Brisbane, Australia. [4]Centre for Clinical Research, The University of Queensland, Brisbane, Australia. [5]Institute for Molecular Bioscience (IMB), IMB Centre for Inflammation and Disease Research, The University of Queensland, Brisbane, Australia. [6]Dept of Respiratory Medicine, Mater Adult Hospital, Brisbane, Australia. [7]Dept of Biomedical Sciences, University of Copenhagen, Copenhagen, Denmark. [8]Contributed equally to this work.

Corresponding author: Katharina Ronacher (katharina.ronacher@mater.uq.edu.au)

Shareable abstract (@ERSpublications)
Viral infections trigger oxysterol production in the lung, attracting macrophages *via* GPR183. Antagonising GPR183 reduced inflammation and disease severity in SARS-CoV-2 infection, making GPR183 a putative target for therapeutic intervention. https://bit.ly/3DXlJCY

Cite this article as: Foo CX, Bartlett S, Chew KY, *et al*. GPR183 antagonism reduces macrophage infiltration in influenza and SARS-CoV-2 infection. *Eur Respir J* 2023; 61: 2201306 [DOI: 10.1183/13993003.01306-2022].

This article has an editorial commentary: https://doi.org/10.1183/13993003.02417-2022

Received: 28 June 2022
Accepted: 20 Oct 2022

Abstract

Rationale Severe viral respiratory infections are often characterised by extensive myeloid cell infiltration and activation and persistent lung tissue injury. However, the immunological mechanisms driving excessive inflammation in the lung remain poorly understood.

Objectives To identify the mechanisms that drive immune cell recruitment in the lung during viral respiratory infections and identify novel drug targets to reduce inflammation and disease severity.

Methods Preclinical murine models of influenza A virus and severe acute respiratory syndrome coronavirus 2 (SARS-CoV-2) infection.

Results Oxidised cholesterols and the oxysterol-sensing receptor GPR183 were identified as drivers of monocyte/macrophage infiltration to the lung during influenza A virus (IAV) and SARS-CoV-2 infection. Both IAV and SARS-CoV-2 infection upregulated the enzymes cholesterol 25-hydroxylase (CH25H) and cytochrome P450 family 7 subfamily member B1 (CYP7B1) in the lung, resulting in local production of the oxidised cholesterols 25-hydroxycholesterol (25-OHC) and 7α,25-dihydroxycholesterol (7α,25-OHC). Loss-of-function mutation of Gpr183 or treatment with a GPR183 antagonist reduced macrophage infiltration and inflammatory cytokine production in the lungs of IAV- or SARS-CoV-2-infected mice. The GPR183 antagonist significantly attenuated the severity of SARS-CoV-2 infection and viral loads. Analysis of single-cell RNA-sequencing data on bronchoalveolar lavage samples from healthy controls and COVID-19 patients with moderate and severe disease revealed that *CH25H*, *CYP7B1* and *GPR183* are significantly upregulated in macrophages during COVID-19.

Conclusion This study demonstrates that oxysterols drive inflammation in the lung *via* GPR183 and provides the first preclinical evidence for the therapeutic benefit of targeting GPR183 during severe viral respiratory infections.

Introduction

Severe viral respiratory infections including influenza and COVID-19 are associated with extensive myeloid cell recruitment to the lung, which can lead to severe tissue injury and the development of acute respiratory distress syndrome [1]. A shift in lung macrophage composition and function is associated with

COVID-19 severity. A study of >600 hospitalised patients found that in severe cases resident alveolar macrophages were depleted and replaced by large numbers of inflammatory monocyte-derived macrophages [2]. Rapid monocyte/macrophage infiltration of the lung during the acute phase of severe acute respiratory syndrome coronavirus 2 (SARS-CoV-2) infection is replicated in animal models [3, 4].

Oxidised cholesterols have recently emerged as markers of inflammation in the lung. Oxysterols were increased in bronchoalveolar lavage fluid (BALF) from inflamed airways after allergen challenge and correlated with infiltrating leukocytes [5]. They were also increased in the sputum from patients with chronic obstructive pulmonary disease, correlating with disease severity [6, 7], and in the lungs of mice after lipopolysaccharide-induced lung inflammation [8]. However, the role of oxysterols in the lung during viral respiratory infections has not been investigated.

Oxysterols have a range of receptors sharing a common role in inflammation [9]. One oxysterol pathway leads to the production of 7α,25-hydroxycholesterol (7α,25-OHC), *via* cholesterol 25-hydroxylase (CH25H) and cytochrome P450 family 7 subfamily B member 1 (CYP7B1) [9, 10]. 7α,25-OHC can subsequently be metabolised by hydroxy-Δ-5-steroid dehydrogenase, 3β- and steroid-Δ isomerase 7 (HSD3B7) (figure 1a). 7α,25-OHC is the endogenous high affinity agonist of the oxysterol-sensing G protein-coupled receptor GPR183 [11, 12]. GPR183 is expressed on cells of the innate and adaptive immune systems, including macrophages, dendritic cells, innate lymphoid cells, eosinophils and T and B lymphocytes [5, 13, 14]. With its oxysterol ligands, GPR183 facilitates the chemotactic distribution of immune cells to secondary lymphoid organs [9, 11, 13, 15]. *In vitro* GPR183 mediates migration of human and mouse macrophages towards a 7α,25-OHC gradient [16, 17].

In this study, we hypothesised that viral respiratory infections lead to the production of oxysterols in the lung, contributing to excessive immune cell infiltration and inflammation. We show that oxysterols drive GPR183-dependent monocyte/macrophage infiltration in preclinical models of influenza virus and SARS-CoV-2 infection and identify GPR183 as a host target for therapeutic intervention to mitigate disease severity in viral respiratory infections.

Methodology

Ethics and biosafety

All experiments were approved by the Animal Ethics Committee (MRI-UQ/596/18, AE000186) and the Institutional Biosafety Committee of the University of Queensland (IBC/465B/MRI/TRI/AIBN/2021).

Viral strains

Virus stocks of A/H1N1/Auckland/1/2009 (H1N1), referred to as influenza A virus (IAV), were prepared in embryonated chicken eggs. A mouse-adapted SARS-CoV-2 strain was obtained through serial passage of SARS-CoV-2 (B.1.351; hCoV-19/Australia/QLD1520/2020, GISAID accession EPI_ISL_968081, collected on 29 December 2020, kindly provided by Queensland Health Forensic and Scientific Services). A description of the mouse-adaption and genomic sequencing data for the SARS-CoV-2 strain can be found in the supplementary methods and figure S1. IAV viral titres were determined by plaque assays on Madin–Darby canine kidney and SARS-CoV-2 plaque assays on Vero E6 cells as described in the supplementary material.

Mouse models

Gpr183^{tm1Lex} were obtained from Lexicon Pharmaceuticals, back-crossed to a C57BL/6J background and bred in-house. 8–10-week-old C57BL/6J and *Gpr183*^{tm1Lex} (*Gpr183*$^{-/-}$) mice were anaesthetised with 4% isoflurane and infected intranasally with 5500 plaque-forming units (PFU) of IAV A/Auckland/01/09 (H1N1). For SARS-CoV-2 infection, C57BL/6J and *Gpr183*$^{-/-}$ mice were anaesthetised with ketamine/xylazine (80 mg·kg^{-1}/5 mg·kg^{-1}) and infected intranasally with 8×10^4 PFU of mouse-adapted SARS-CoV-2. Lungs were collected at specified time points for subsequent downstream analysis as described in the supplementary material. The GPR183 antagonist NIBR189 (7.6 mg·kg^{-1}) in vehicle (0.5% carboxymethylcellulose/0.5% Tween-80) or vehicle only was administrated by oral gavage from 1 day post infection (dpi), twice daily at 12-h intervals until the end of the experiment.

RNA isolation and reverse-transcriptase quantitative PCR

Total RNA was isolated using the ISOLATE II RNA Mini Kit (Bioline Reagents Ltd.), as previously described [18, 19]. The list of primers is provided in supplementary table S1. The relative expression of each gene normalised to the reference gene hypoxanthine-guanine phosphoribosyltransferase (*Hprt*) was determined using the $2^{-\Delta Ct}$ method.

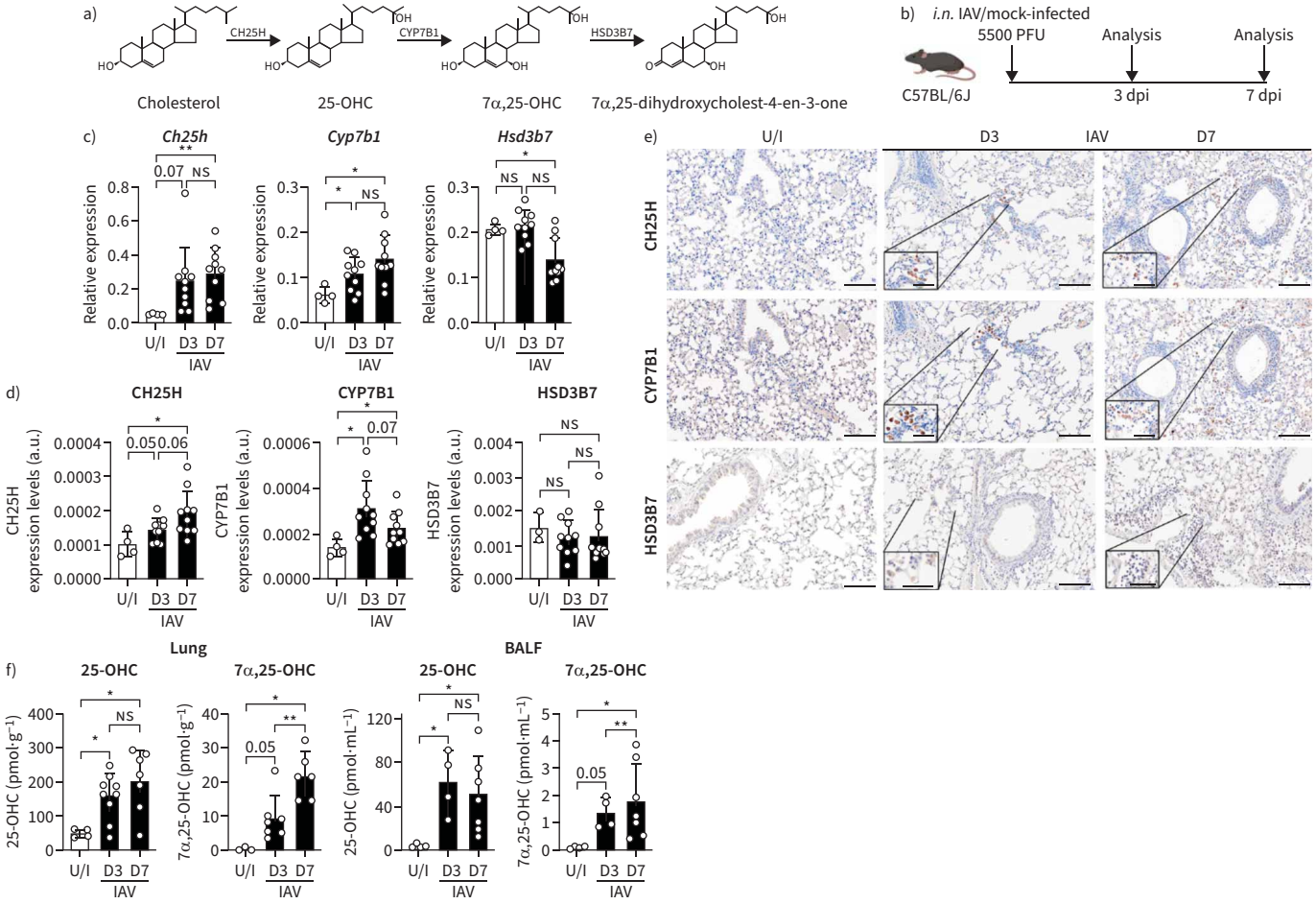

FIGURE 1 Influenza A virus (IAV) infection leads to upregulation of cholesterol 25-hydroxylase (CH25H) and cytochrome P450 family 7 subfamily member B1 (CYP7B1) expression in the lung and production of the oxysterols 25-hydroxycholesterol (25-OHC) and 7α,25-dihydroxycholesterol (7α,25-OHC). a) The biosynthetic pathway of 25-OHC and 7α,25-OHC. b) Experimental design: C57BL/6J mice were infected intranasally (*i.n.*) with 5500 plaque-forming units (PFU) of IAV. c) mRNA expression of *Ch25h*, *Cyp7b1* and *Hsd3b7* was measured by quantitative reverse transcription PCR at 3 days post infection (dpi) (D3) and 7 dpi (D7) normalised to *Hprt*. d) Quantitative analysis of CH25H, CYP7B1 and HSD3B7 protein labelling by immunohistochemistry (IHC). e) Representative IHC images of CH25H, CYP7B1 and HSD3B7 in lung sections of uninfected or IAV-infected mice. Scale bars: 100 µm (main) and 50 µm (inset). f) Concentrations of 25-OHC and 7α,25-OHC in the lungs (left) and bronchoalveolar lavage fluid (BALF) (right) at 3 dpi and 7 dpi. Data are presented as mean±SD of n=4 uninfected and n=6–10 infected mice per time point. NS: nonsignificant; U/I: mock infected. *: p<0.05; **: p<0.01.

Oxysterol extraction and mass spectrometric quantitation

The oxysterol extraction and quantification methods were adapted from Ngo *et al*. [18] as described in the supplementary material.

Cytokine quantification using ELISA

Cytokines in lung homogenates were measured with DuoSet ELISA (interferon (IFN) β (DY8234-05), IFNγ (DY485), IFNλ (DY1789B), interleukin (IL) 6 (DY406), tumour necrosis factor α (TNFα) (DY410), IL-1β (DY401), IL-10 (DY417) and CC motif chemokine ligand 2 (CCL2) (DY479); R&D Systems) according to the manufacturer's protocol.

Flow cytometry

Flow cytometry was performed on single-cell suspensions from digested lungs and blood as described in detail in the supplementary material.

Immunohistochemistry

Immunohistochemistry (IHC) was performed on deparaffinised/rehydrated lung sections by immunolabelling with antibodies against SARS-CoV-2 nucleocapsid protein (40143-R040; Sino

Biological), ionised calcium-binding adapter molecule 1 (IBA1) (019-19741; NovaChem), CH25H (BS-6480R; Bioss Antibodies), CYP7B1 (BS-5052R; Bioss Antibodies) and isotype control (rabbit IgG; 31235; Thermo Fisher Scientific) diluted in Da Vinci Green Diluent (PD900; Biocare Medical), followed by incubation with horseradish peroxidase-conjugated goat anti-rabbit Ig antibody (1:200) (ab6721; Abcam) (supplementary material). Isotype controls are shown in supplementary figure S2.

Statistical analysis

Data were analysed on GraphPad Prism software. Data were assessed for normality using a Shapiro–Wilk test. Spearman's rank correlation was used to analyse correlations. For two group comparisons, a parametric two-tailed t-test was used for normally distributed data while a non-parametric Mann–Whitney U test was used for data that deviated from normality.

Results

IAV infection increases CH25H and CYP7B1 expression and oxysterol production in the lung

To investigate whether IAV infection induces the production of oxidised cholesterols, mice were infected with IAV (figure 1b) and mRNA expression of oxysterol-producing enzymes was determined in lung tissue. *Ch25h* and *Cyp7b1* mRNA were increased in lungs of IAV-infected mice compared to uninfected animals, whereas *Hsd3b7* was downregulated in the lung 7 dpi (figure 1c). Similarly, CH25H and CYP7B1 proteins were also increased while HSD3B7 remained constant, as demonstrated by immunohistochemical labelling of lung sections with antibodies detecting CH25H, CYP7B1 and HSD3B7 (figure 1d, e). The induction of oxysterol-producing enzymes was associated with increased concentrations of the oxysterols 7α,25-OHC and 25-OHC in lung homogenates (figure 1f, left panels) and BALF (figure 1f, right panels) from IAV-infected animals at both 3 dpi and 7 dpi. In uninfected lungs, 7α,25-OHC was undetectable in most samples tested. *Ch25h* and *Cyp7b1* mRNA were increased in the bronchoalveolar lavage (BAL) cell pellet of IAV-infected mice compared to uninfected animals while *Hsd3b7* remained unchanged (supplementary figure S3a).

Consistent with the increase in oxysterols, *Gpr183* mRNA was increased at 3 dpi and 7 dpi in both BAL cells (supplementary figure S3a) and lung tissue (supplementary figure S3b), suggesting increased expression and/or recruitment of GPR183-expressing immune cells to the lung upon infection. *Gpr183* expression was positively correlated with *Ch25h* and *Cyp7b1* (supplementary figure S3c).

Gpr183$^{-/-}$ *mice have reduced macrophage infiltration into the lungs upon IAV infection*

To investigate whether oxysterol-mediated immune cell recruitment is dependent on the oxysterol-sensing GPR183, we performed experiments in mice genetically deficient in *Gpr183* (*Gpr183*$^{-/-}$). *Gpr183*$^{-/-}$ mice exhibit normal gross phenotype [20], and had normal circulating monocyte numbers and comparable numbers of macrophage colony forming units in the bone marrow to C57BL/6 mice (supplementary figure S4), suggesting comparable monopoiesis in *Gpr183*$^{-/-}$ mice. However, upon infection with IAV, *Gpr183*$^{-/-}$ mice had lower IBA1^{+} macrophage numbers in the lung at 3 dpi and 7 dpi than infected C57BL/6J controls (figure 2a). *Gpr183* expression was positively correlated with mRNA expression of the pro-inflammatory cytokines *Il6*, *Tnf* and *Ccl2* in C57BL/6J mice (supplementary figure S5), and reduced macrophage infiltration in *Gpr183*$^{-/-}$ mice was associated with reduced *Il6* and *Tnf*, but not *Ccl2*, at 7 dpi (supplementary figure S6). Body weights and viral titres through the course of IAV infection were comparable across the genotypes (supplementary figure S7). These results demonstrate that lack of GPR183 reduces macrophage infiltration into the lung upon IAV infection, which is associated with reduced pro-inflammatory cytokine expression.

GPR183 antagonism reduces macrophage infiltration

To investigate whether GPR183 is a putative therapeutic target to reduce inflammation, the GPR183 antagonist NIBR189 [11, 17] was administered to C57BL/6J mice twice daily starting from 24 h post infection until the end of the experiment (figure 2b). Like *Gpr183*$^{-/-}$ mice, C57BL/6J animals treated with NIBR189 had significantly reduced macrophage infiltration into the lung both at 3 dpi and 7 dpi as determined by IHC (figure 2c).

In addition, flow cytometry analysis was performed on lung single-cell suspensions from C57BL/6J and *Gpr183*$^{-/-}$ mice treated with NIBR189 and vehicle, respectively, using a previously published gating strategy (supplementary figure S8) [21]. NIBR189-treated C57BL/6J mice and *Gpr183*$^{-/-}$ mice had lower percentages of recruited/infiltrated macrophages (F480^{high}/CD11b^{+}/Ly6G^{-}/SigF^{-}) (figure 3a) compared to vehicle-treated C57BL/6J animals after IAV infection. NIBR189 treatment did not change the percentages of other immune cell subsets in the lung, including neutrophils (B220^{-}/CD3^{-}/Ly6G^{+}/CD11b^{+}) (figure 3a), CD4^{+} T-cells, CD8^{+} T-cells, B-cells, dendritic cells and alveolar macrophages (supplementary figures S9

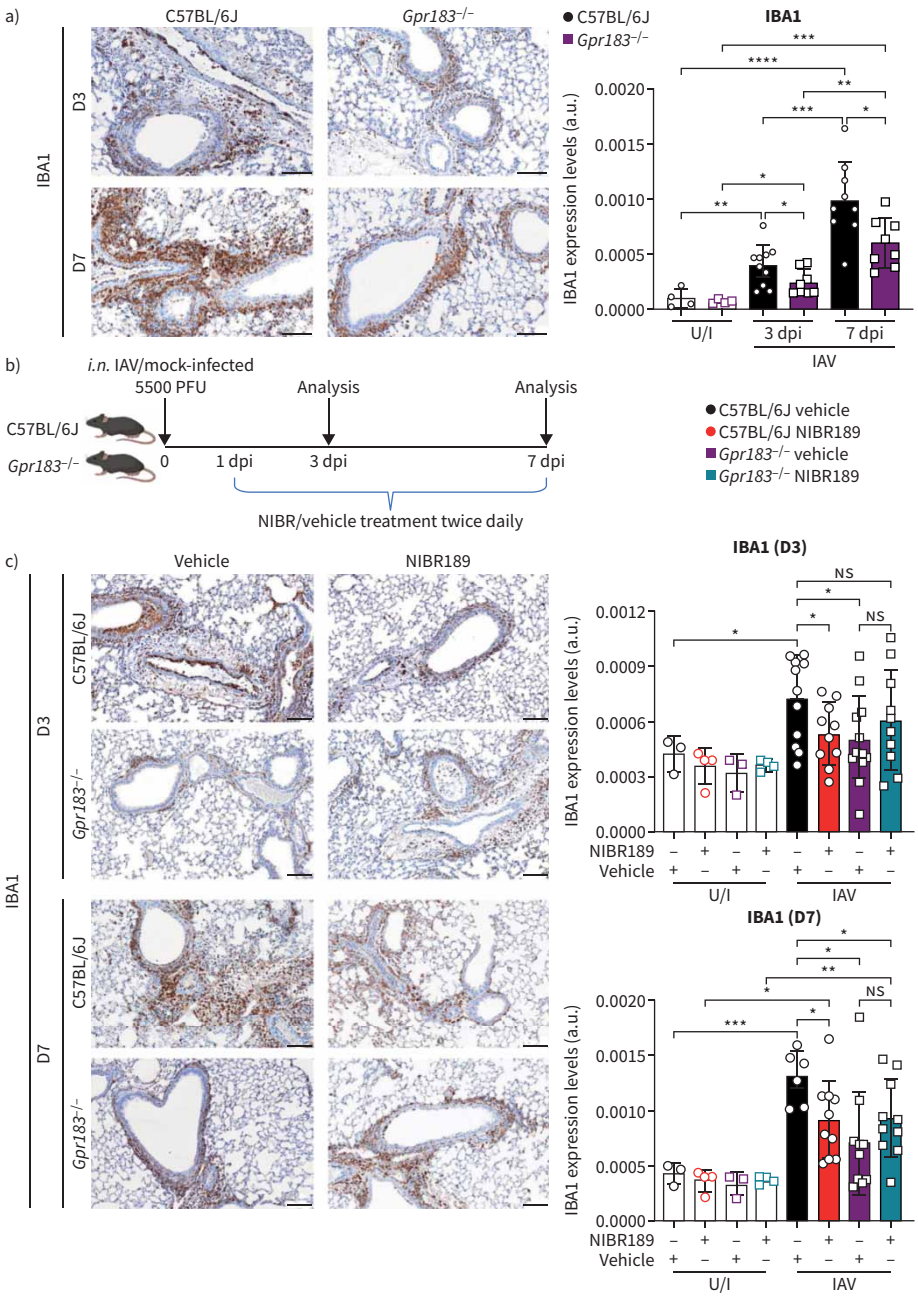

FIGURE 2 Deletion of the *Gpr183* gene or administration of a GPR183 antagonist reduces macrophage infiltration in influenza A virus (IAV)-infected lungs. C57BL/6J and *Gpr183*$^{-/-}$ mice were infected intranasally with 5500 plaque-forming units (PFU) of IAV. a) Representative immunohistochemistry (IHC) images of ionised calcium-binding adapter molecule 1 (IBA1) in lung sections of IAV-infected C57BL/6J and *Gpr183*$^{-/-}$ mice (left) and quantitative analysis (right). b) Experimental design: C57BL/6J mice and *Gpr183*$^{-/-}$ mice were infected intranasally (*i.n.*) with 5500 PFU of IAV. Mice were subsequently treated orally with 7.6 mg·kg^{-1} NIBR189 or vehicle control twice daily from 1 day post infection (dpi) until the end of the experiment. c) Representative IHC images of IBA1 in lung sections of C57BL/6J and *Gpr183*$^{-/-}$ mice with the respective treatment groups at 3 dpi (D3) and 7 dpi (D7) (left) and quantitative analysis of IBA1 staining (right). Data are presented as mean±SD of n=6–12 infected mice per genotype and time point. Scale bars: 100 µm. a.u.: arbitrary units; U/I: mock infected; NS: nonsignificant. *: p<0.05; **: p<0.01; ***: p<0.001; ****: p<0.0001.

and S10). Body weights and lung viral loads were not affected by genotype or treatment (supplementary figure S11).

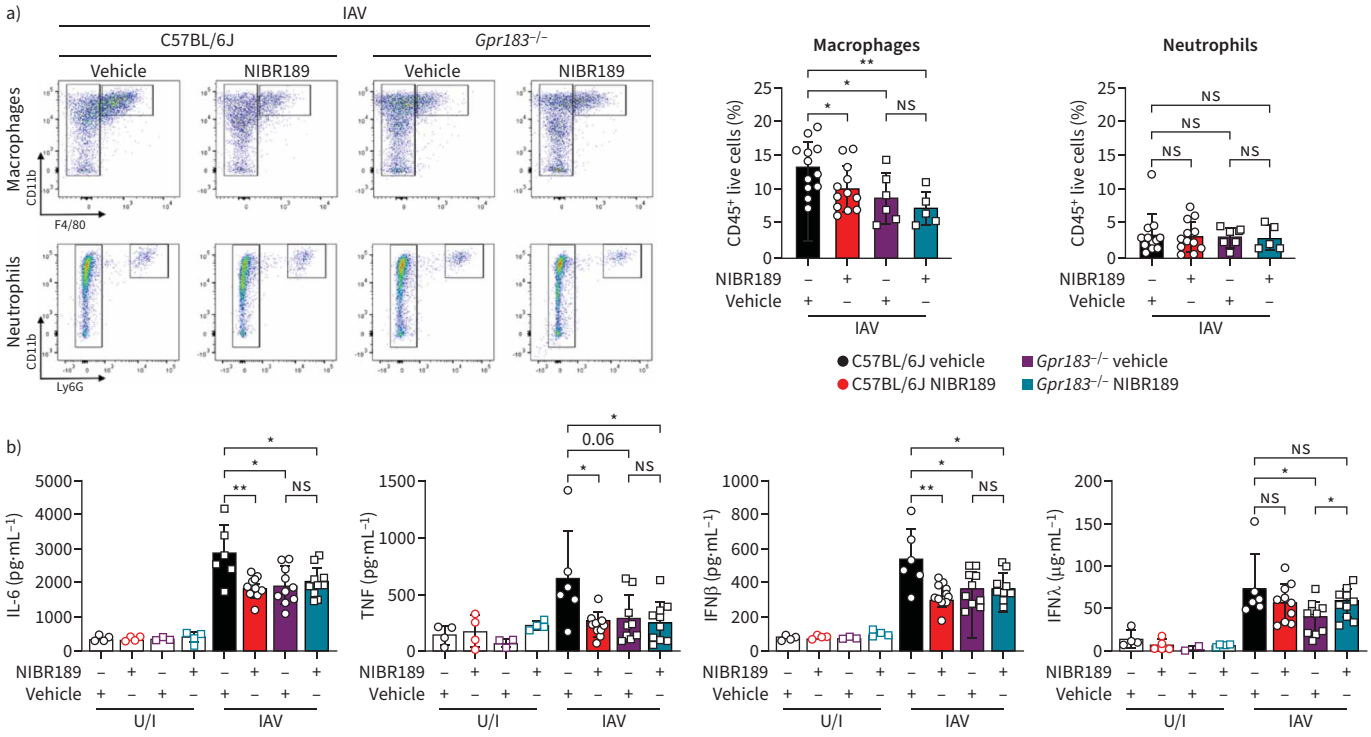

FIGURE 3 The GPR183 antagonist NIBR189 reduces macrophage infiltration and inflammatory cytokine production. C57BL/6J and *Gpr183*$^{-/-}$ mice were infected intranasally with 5500 plaque-forming units (PFU) of influenza A virus (IAV). Mice were subsequently treated orally with 7.6 mg·kg^{-1} NIBR189 or vehicle control twice daily from 1 day post infection (dpi) until the end of the experiment. a) Frequency of infiltrating macrophages (F480^{high}/CD11b^{+}/Ly6G^{-}/SigF^{-}) and neutrophils (B220^{-}CD3^{-}Ly6G^{+}) was determined by flow cytometry relative to total viable CD45^{+} immune cells at 3 dpi (left). Graphs show the frequency of macrophages and neutrophils (right). b) Cytokine measurements of interleukin 6 (IL-6), tumour necrosis factor (TNF), interferon β (IFNβ) and interferon λ (IFNλ) at 7 dpi measured by ELISA. Data are presented as mean±SD of n=5–12 infected mice per genotype and time point. U/I: mock infected; NS: nonsignificant. *: p<0.05; **: p<0.01.

These results demonstrate that NIBR189 significantly reduced macrophage infiltration to the lung without affecting the recruitment of other immune cell subsets.

GPR183 antagonism reduces IAV-induced pro-inflammatory cytokine concentrations

We next determined if the reduced macrophage infiltration mediated by NIBR189 results in reduced inflammatory cytokine production in the lung. At 3 dpi, no significant differences in cytokine production were observed between treatment groups (supplementary figure S12). However, IAV-infected C57BL/6J mice treated with NIBR189 had significantly lower concentrations of IL-6, TNF and IFNβ (figure 3b) at 7 dpi. This was comparable to the phenotype of IAV-infected *Gpr183*$^{-/-}$ mice, with NIBR189 treatment having no additional effect in mice deficient in GPR183. In addition, no significant differences were observed in IFNλ across the two time points (figure 3b and supplementary figure S12), demonstrating that GPR183 antagonist treatment does not negatively impact the production of type III IFNs, which are important for viral control in the lung [22]. No differences between treatment groups were observed at either time point for protein concentrations of IL-1β, CCL2 or IFNγ between treatment groups (supplementary figures S12 and S13). Thus, GPR183 can be inhibited pharmacologically to reduce pro-inflammatory cytokines upon severe IAV infection.

GPR183 antagonism reduces SARS-CoV-2 infection severity

Excessive macrophage infiltration and activation is a hallmark of severe COVID-19 [2, 23]. To evaluate whether the benefits of inhibiting GPR183 extend to SARS-CoV-2 infection, we established a mouse-adapted SARS-CoV-2 strain by passaging the Beta variant of SARS-CoV-2 (B.1.351) four times in C57BL/6J mice. This resulted in a virus that contained a mutation in non-structural protein 5 (NSP5) and caused clinical signs (weight loss) in infected mice (supplementary figure S1). Consistent with the IAV infection results, mRNA expression of *Ch25h* and *Cyp7b1* was significantly upregulated in the lungs of SARS-CoV-2-infected mice compared to uninfected mice while *Hsd3b7* remained unchanged (figure 4a).

This was confirmed also at the protein level by IHC (figure 4b, c). Further, 25-OHC and 7α,25-OHC concentrations in lung homogenates (figure 4d, top panels) and BALF (figure 4d, bottom panels) were significantly increased at 2 dpi, returning to uninfected levels by 5 dpi by which time the animals began to recover from the infection. *Ch25h* and *Gpr183* were also increased in BAL cells of SARS-CoV-2-infected mice while *Hsd3b7* remained unchanged (supplementary figure S14). NIBR189 or vehicle was administered to C57BL/6J or *Gpr183*$^{-/-}$ mice twice daily from 24 h post-SARS-CoV-2 infection until the end of the experiment (figure 5a). NIBR189-treated C57BL/6J mice lost significantly less weight and recovered faster compared to vehicle-treated mice (figure 5b and supplementary figure S15). Similarly, *Gpr183*$^{-/-}$ mice had less severe SARS-CoV-2 infection. Collectively, these data demonstrate that oxysterols are produced in the lung upon SARS-CoV-2 infection and GPR183 antagonism significantly reduced SARS-CoV-2 infection severity.

GPR183 antagonism reduces macrophage infiltration and inflammatory cytokine expression in the lung of SARS-CoV-2 infected mice

Next, we investigated whether GPR183 antagonism decreases macrophage infiltration and inflammatory cytokines in the lung. SARS-CoV-2-infected C57BL/6J mice treated with NIBR189 had significantly reduced macrophage infiltration into the lung at 2 dpi and 5 dpi (figure 5c, d). NIBR189 treatment was associated with reduced *Tnf*, *Il10* and *Ifng* mRNA expression at 2 dpi (figure 6a and supplementary figure S16), and reduced *Tnf, Il1b and Il6* expression at 5 dpi (figure 6b and supplementary figure S16). Early IFN responses were not affected by NIBR189, with comparable *Ifnb* and *Ifnl* expression at 2 dpi in C57BL/6J mice, but late IFN responses (5 dpi) were significantly lower in NIBR-treated animals compared to controls (figure 6). No differences between treatment groups were observed for mRNAs encoding *Ccl2*, *Il1b* or *Il6* at 2 dpi and *Ccl2*, *Il10* and *Ifng* at 5 dpi (supplementary figure S16). These results demonstrate that reduced macrophage infiltration in NIBR189-treated mice was associated with reduced pro-inflammatory cytokine expression in the lung, while the early antiviral IFN responses remained unchanged.

GPR183 antagonism reduces SARS-CoV-2 loads

Finally, we investigated whether NIBR189 treatment is associated with altered viral loads. SARS-CoV-2 nucleocapsid protein expression was reduced in NIBR189-treated C57BL/6J mice compared to those

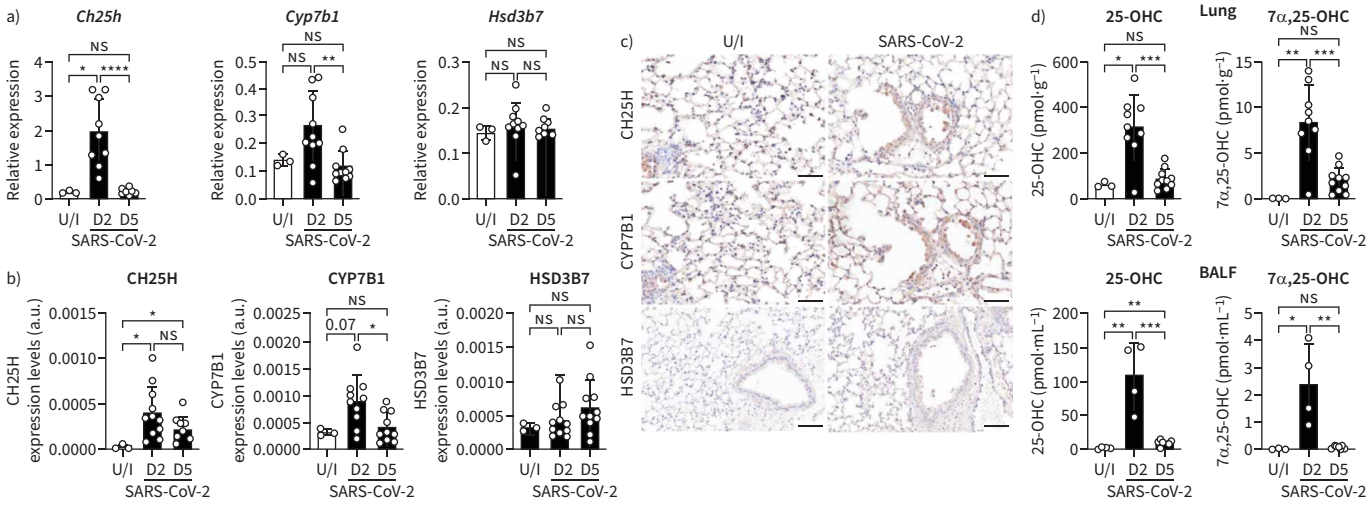

FIGURE 4 Severe acute respiratory syndrome coronavirus 2 (SARS-CoV-2) infection leads to upregulation of cholesterol 25-hydroxylase (CH25H) and cytochrome P450 family 7 subfamily member B1 (CYP7B1) expression in the lung and production of the oxysterols 25-hydroxycholesterol (25-OHC) and 7α,25-dihydroxycholesterol (7α,25-OHC). C57BL/6J mice were infected intranasally with approximately 8×10^4 plaque-forming units (PFU) of mouse49-adapted SARS-CoV-2. mRNA expression of a) *Ch25h*, *Cyp7b1* and *Hsd3b7* was measured by quantitative reverse transcription PCR at 2 days post infection (dpi) (D2) and 5 dpi (D5) normalised to *Hprt*. b) Quantitative analysis of CH25H, CYP7B1 and HSD3B7 protein by immunohistochemistry (IHC) labelling at D2 and D5 and c) representative IHC images of CH25H, CYP7B1 and HSD3B7 in lung sections in uninfected mice at D2. d) Concentrations of 25-OHC and 7α,25-OHC in the lungs (top) and bronchoalveolar lavage fluid (BALF) (bottom) at D2 and D5. Data are presented as mean±SD of n=3 uninfected mice and n=9–10 infected mice per time point. Scale bars: 50 µm. U/I: mock infected; a.u.: arbitrary units; NS: nonsignificant. *: p<0.05; **: p<0.01; ***: p<0.001; ****: p<0.0001.

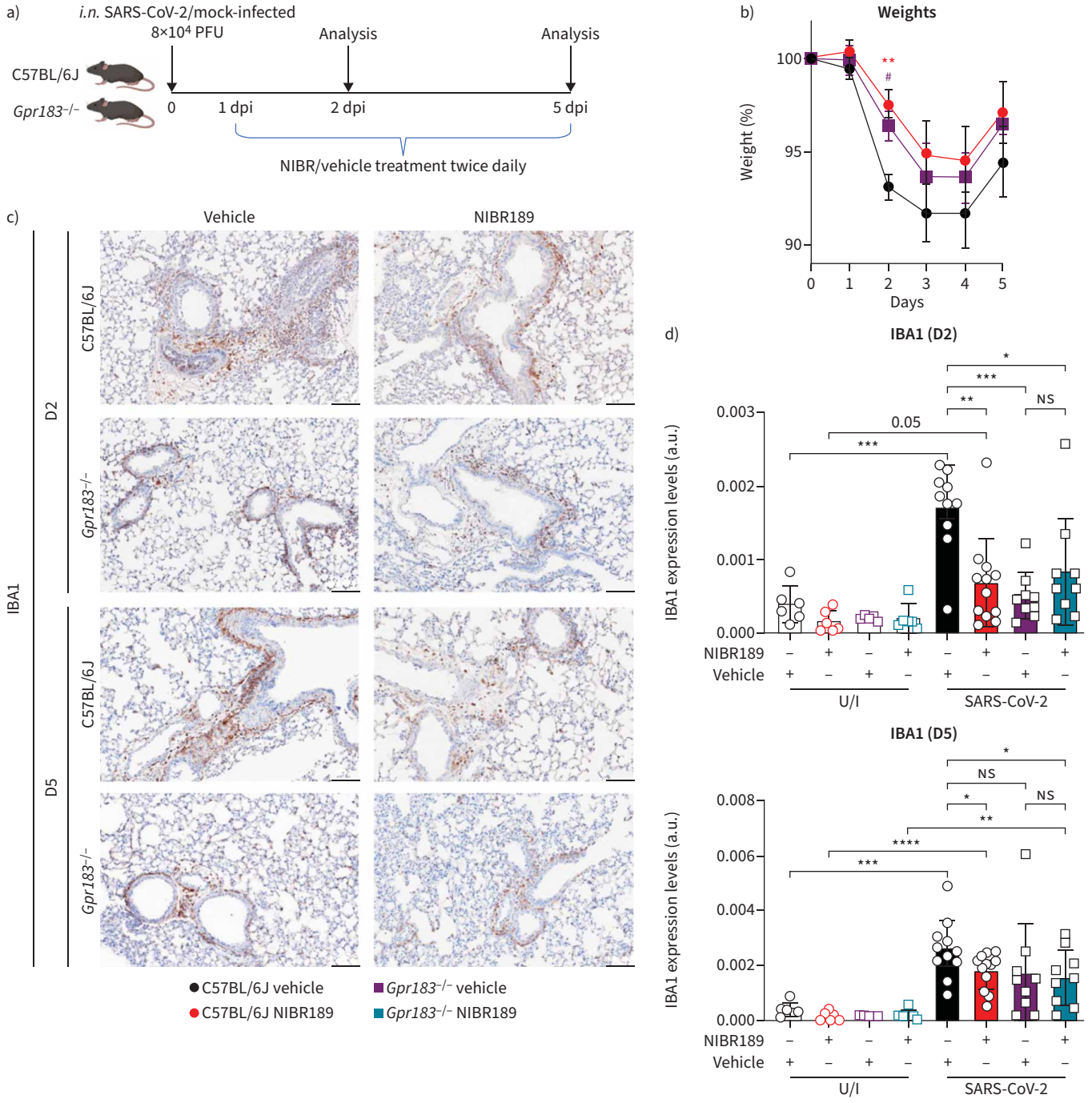

FIGURE 5 GPR183 antagonism resulted in less severe acute respiratory syndrome coronavirus 2 (SARS-CoV-2) infection-induced weight loss and in reduced macrophage infiltration. C57BL/6J and *Gpr183*$^{-/-}$ mice were infected intranasally with approximately 8×10^4 plaque-forming units (PFU) of mouse-adapted SARS-63 CoV-2. Mice were subsequently treated orally with 7.6 mg·kg^{-1} NIBR189 or vehicle control twice daily from 1 day post infection (dpi) until the end of the experiment. a) Experimental design. b) Weights of mice displayed as percentage of the weight at time of inoculation. c) Representative immunohistochemistry (IHC) images of ionised calcium-binding adapter molecule 1 (IBA1) in lung of C57BL/6J and *Gpr183*$^{-/-}$ mice with the respective treatment groups at 2 dpi (D2) and 5 dpi (D5). Scale bars: 100 µm. d) Quantitative analysis of IBA1 at D2 and D5. Data are presented as mean±SD of n=9–12 infected mice per genotype and time point. a.u.: arbitrary units; U/I: uninfected; NS: nonsignificant. *: p<0.05; **: p<0.01; ***: p<0.001.

administered vehicle at 2 dpi (figure 7a, b). Nucleocapsid protein expression was not detected at 5 dpi, when the animals recovered from the infection. However, at the mRNA level, viral *Mpro* RNA loads in the lungs of NIBR189-treated mice were significantly lower at 5 dpi (figure 7c). Corroborating this, viral PFUs

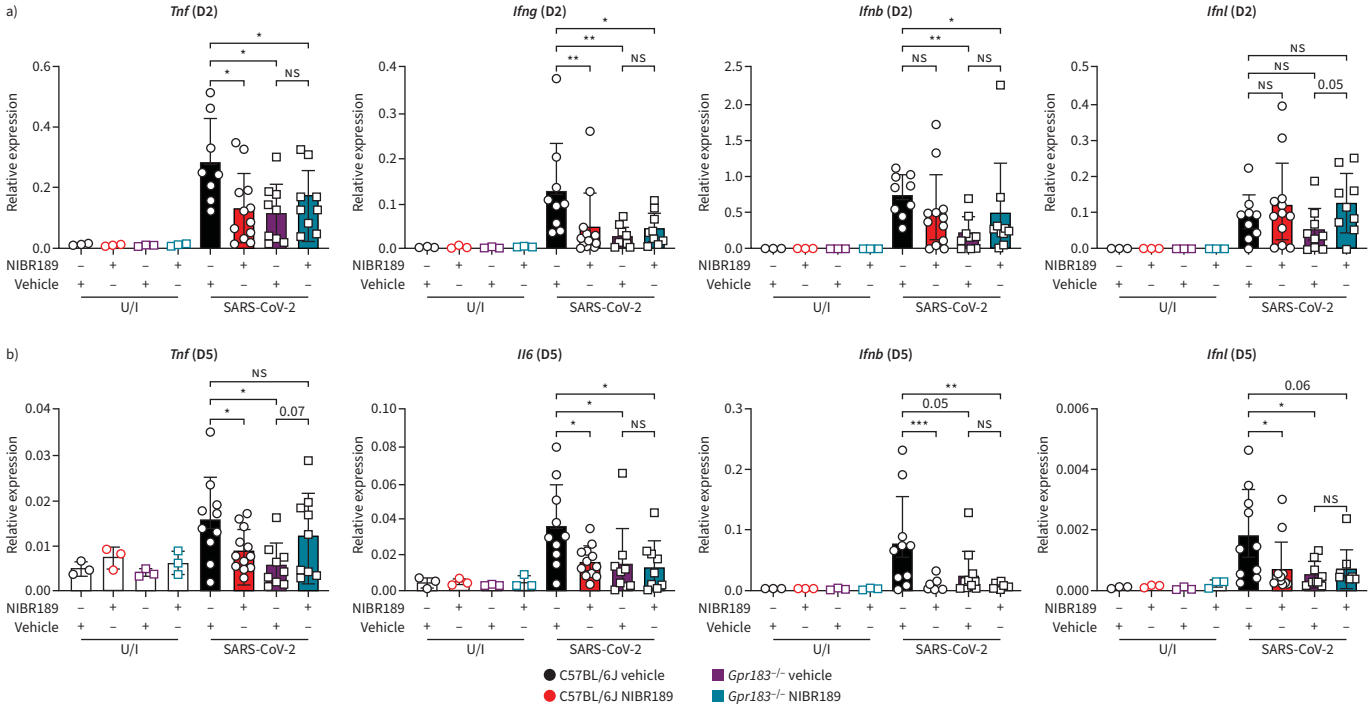

FIGURE 6 GPR183 antagonism led to a reduced inflammatory cytokine profile. C57BL/6J and *Gpr183*$^{-/-}$ mice were infected intranasally with approximately 8×10^4 plaque-forming units (PFU) of mouse-adapted severe acute respiratory syndrome coronavirus 2 (SARS-CoV-2). Mice were subsequently treated orally with 7.6 mg·kg^{-1} NIBR189 or vehicle control twice daily from 1 day post infection (dpi) until the end of the experiment. Relative expression of *Tnf*, *Ifng*, *Ifnb and Ifnl* at a) 2 dpi (D2) and b) 5 dpi (D5) in the lungs measured by reverse transcription quantitative PCR, normalised to *Hprt*. Data are presented as mean±SD of n=3 uninfected mice and n=9–12 infected mice per genotype and time point. U/I: mock infected; NS: nonsignificant. *: p<0.05; **: p<0.01; ***; p<0.001.

were significantly lower at both 2 dpi and 5 dpi in NIBR-treated animals (supplementary figure S17). In summary, we demonstrate here that GPR183 antagonism reduces viral loads, macrophage infiltration and production of pro-inflammatory cytokines in SARS-CoV-2 infection.

Lung macrophages from COVID-19 patients upregulate CH25H, CYP7B1, HSD3B7 *and* GPR183

To determine whether the oxysterol-producing enzymes are increased in humans during SARS-CoV-2 infection, we analysed single-cell RNA-sequencing (scRNA-seq) data from healthy controls and COVID-19 patients with moderate and severe disease [23]. We found that *CH25H*, *CYP7B1* and *HSD3B7* were significantly upregulated in COVID-19 and almost exclusively expressed in macrophages (figure 8). While *GPR183* expression increased significantly in macrophages and myeloid dendritic cells during COVID-19, its expression remained unchanged in other immune cell types.

Discussion

We report that 25-OHC and 7α,25-OHC are produced in the lung upon IAV or SARS-CoV-2 infection, attracting monocytes/macrophages in a GPR183-dependent manner. Reduced macrophage infiltration and inflammatory cytokine production in *Gpr183*$^{-/-}$ mice and NIBR189-treated C57BL/6J mice significantly improved SARS-CoV-2 infection severity. The antagonist attenuated SARS-CoV-2 but not IAV loads. Whether this is due to pathogen-specific effects or due to more severe disease observed in the IAV model compared to the SARS-CoV-2 model remains to be investigated. However, macrophage infiltration and inflammatory cytokine production were reduced in both viral models.

In animal models of IAV and SARS-CoV-2, myeloid cells rapidly infiltrate into the lungs [3, 4, 24]. Patients with severe COVID-19 have higher proportions of GPR183$^+$ macrophages and more activated macrophages in BALF [23], strongly implicating macrophages as key contributors to COVID-19-associated hyperinflammation. BALF from severe COVID-19 patients is enriched in the chemokines CCL2 and CCL7, which recruit monocytes to the lung *via* the chemokine receptor C-C motif chemokine receptor 2 (CCR2) [25]. Historically, chemokines have been considered the main drivers of immune cell migration

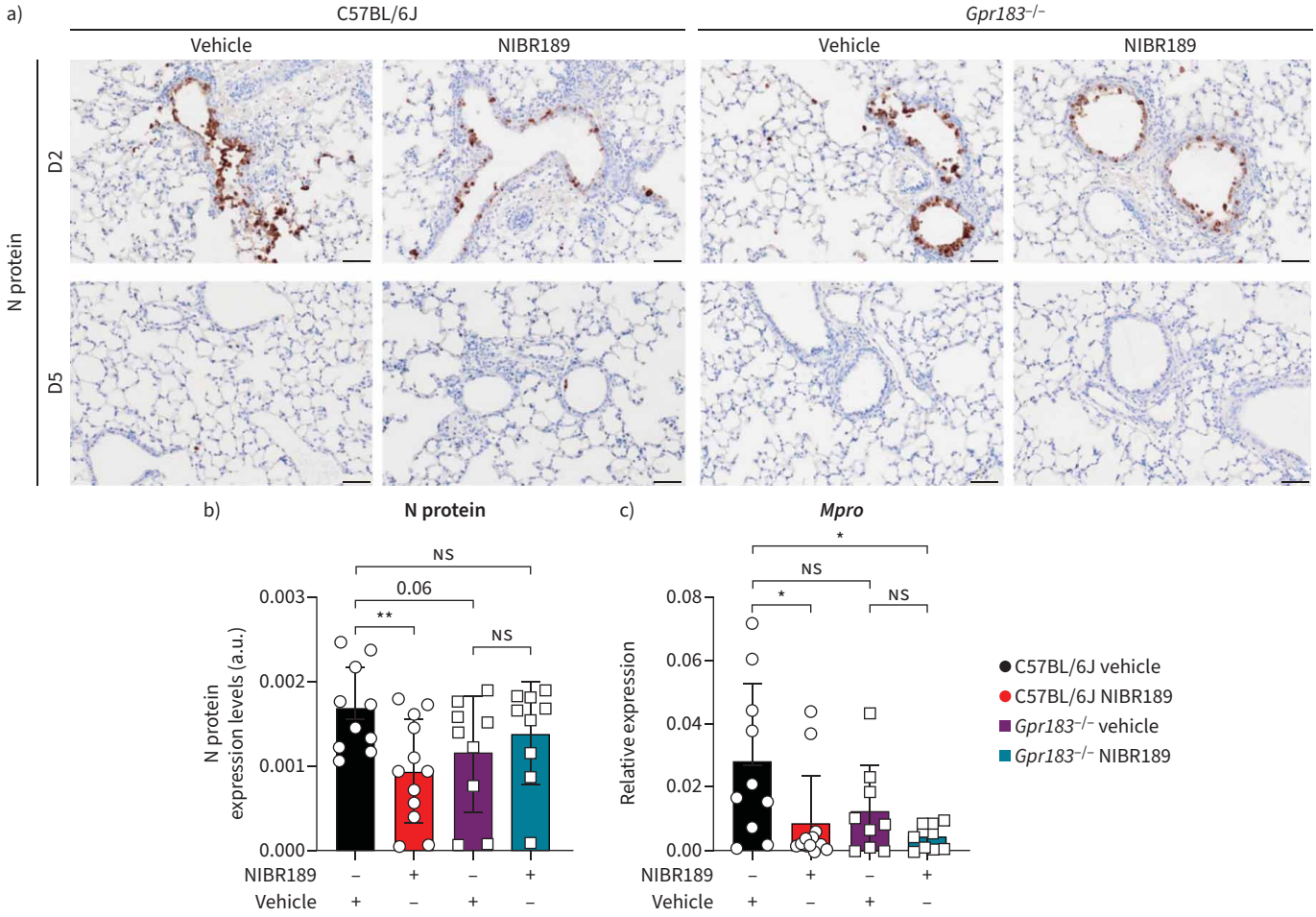

FIGURE 7 Mice treated with GPR183 antagonist had lower severe acute respiratory syndrome coronavirus 2 (SARS-CoV-2) loads. C57BL/6J and *Gpr183*$^{-/-}$ mice were infected intranasally with approximately 8×10^{4} plaque-forming units (PFU) of mouse-adapted SARS-CoV-2. Mice were subsequently treated orally with 7.6 mg·kg^{-1} NIBR189 or vehicle control twice daily from 1 day post infection (dpi) until the end of the experiment. a) Representative immunohistochemistry (IHC) images of viral nucleocapsid (N protein) expression at 2 dpi (D2) and 5 dpi (D5). b) Quantitative analysis of viral N protein expression of the treatment groups at D2. c) Viral load was assessed in the lung through the detection of *Mpro* RNA by reverse transcription quantitative PCR at D5, normalised to *Hprt*. Data are presented as mean±SD of n=9–12 infected mice per genotype and time point. Scale bars: 50 µm. a.u.: arbitrary units; U/I: mock infected; NS: nonsignificant. *: p<0.05; **: p<0.01.

into the lung; however, our work here reveals that oxysterols have a nonredundant role in monocyte/macrophage infiltration. We further demonstrate that lung macrophages from COVID-19 patients express higher levels of the oxysterol-producing enzymes and GPR183, indicating that this mechanism is conserved in humans. Similar to our observations in *Gpr183*$^{-/-}$ mice, mice lacking CCR2 have delayed macrophage infiltration into the lung [21]; however, CCR2 is also required for T-cell migration. Therefore, animals lacking CCR2 had delayed T-cell infiltration and higher viral titres [26]. Although GPR183 is expressed in T-cells, it is not essential for T-cell migration into the lung [27] and antagonising GPR183 did not negatively impact the T-cell compartment nor other immune cell subsets.

We recently showed in a murine model of *Mycobacterium tuberculosis* (Mtb) infection that both GPR183 and the 7α,25-OHC-producing enzyme CYP7B1 are required for rapid macrophage infiltration into the lung upon mycobacterial infection [18]. In the Mtb model, GPR183 is also required for infiltration of eosinophils [14]. We identified both alveolar macrophages and infiltrating macrophages as the predominant cell types expressing CH25H and CYP7B1 upon Mtb infection [18] and corroborated this here with the scRNA-seq data from COVID-19 patients.

Deletion of *Ch25h* has previously been shown to be protective in a mouse model of influenza [28]. 25-OHC was increased in a model of acute lung injury; however, it was decreased in a house dust

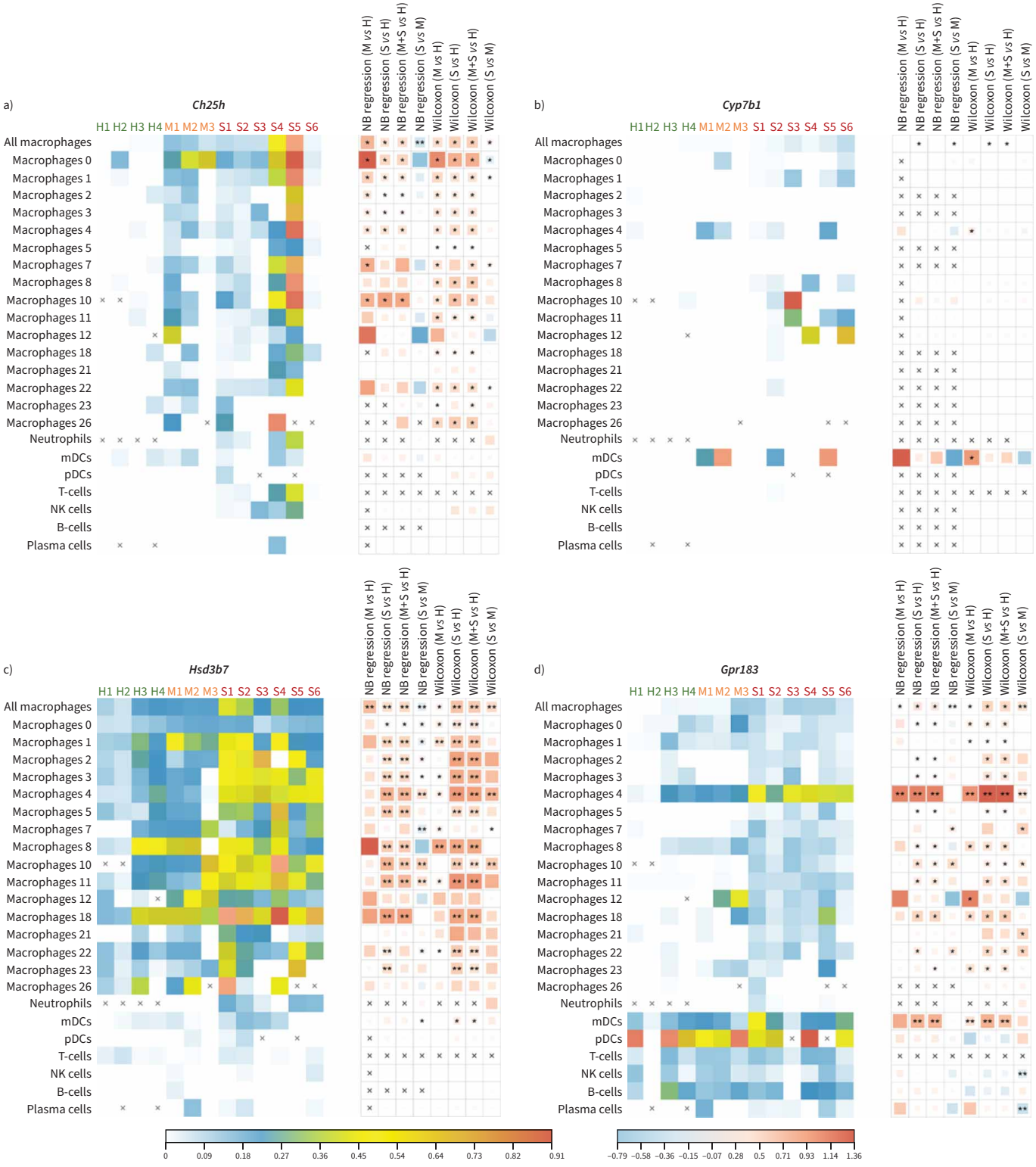

FIGURE 8 Single-cell RNA-sequencing expression analysis of cells collected by bronchoalveolar lavage from healthy controls and COVID-19 patients. Summary heatmaps in the left panels show average normalised expression level of genes a) *Ch25h*, b) *Cyp7b1*, c) *Hsd3b7* and d) *Gpr183* per individual per cell type cluster. Summary heatmaps in the right panels show the average log fold change (logFC) in expression of each gene in 24 cell type clusters between moderate COVID-19 cases and healthy controls (M *vs* H), severe COVID-19 cases and healthy controls (S *vs* H), COVID-19 cases and healthy controls (M+S *vs* H), and severe and moderate COVID-19 cases (S *vs* M).The logFC values were estimated using negative binomial generalised linear models applied to raw UMI counts, adjusting for total UMI counts per cell, number of genes detected per cell and per cent mitochondrial counts per cell (NB regression); or non-parametric Wilcoxon rank sum test applied to normalised counts. Significant

associations are highlighted with a single asterisk if they surpass Bonferroni significance ($p<1.30\times10^{-4}$) or a double asterisk if they were further expressed in at least 5% of cells in both groups with an absolute value of logFC >0.25. A logFC >0 suggests the expression level of the gene is higher among the focal group (*e.g.* moderate COVID-19 cases) compared to the other group (*e.g.* healthy controls), or vice versa. mDC: myeloid dendritic cell; pDC: plasmacytoid dendritic cell; NK: natural killer.

mite-induced model of asthma [8]. Intratracheal administration of 25-OHC improved inflammatory markers in the acute lung injury model, whereas it worsened the hallmarks of the asthma model. In both models, *Gpr183* expression was unaffected. This suggests that 25-OHC production is model specific.

Here we show that reduced macrophage infiltration in *Gpr183*$^{-/-}$ mice and NIBR189-treated C57BL/6J mice was associated with reduced pro-inflammatory cytokine production, likely due to lower numbers of macrophages present in the tissue. Although we did not observe a NIBR189-mediated reduction in *Tnf*, *Il6* or *Ifnb* expression in IAV-infected or lipopolysaccharide-stimulated bone marrow-derived macrophages (supplementary figure S18), we cannot completely exclude a direct effect of NIBR189 on cytokine production by other immune cells. Irrespective of the exact mechanism, lower pro-inflammatory cytokine production in NIBR189-treated animals may explain, at least in part, the better disease outcomes.

While pro-inflammatory cytokines can be detrimental to the host [29], early type I and III IFNs are crucial in controlling viral replication during IAV [30, 31] and SARS-CoV-2 infection [32, 33]. NIBR189 did not alter early type I or III IFN responses in SARS-CoV-2-infected animals, suggesting that the antiviral response was not impaired by the treatment.

Several oxysterols can have a direct antiviral effect [9]. CH25H/25-OHC have been shown to inhibit SARS-CoV-2 infection *in vitro* by blocking the virus–host cell membrane fusion [34, 35]. Whether NIBR189, which is structurally different from oxysterols, affects viral entry/replication remains to be elucidated.

Other immunosuppressive therapies used in severe COVID-19, like glucocorticoids, increase angiotensin-converting enzyme 2 (ACE2) expression, which promotes viral entry/replication [36, 37] and delays SARS-CoV-2 clearance [38]. NIBR189 did not increase *Ace2* mRNA (supplementary figure S19),

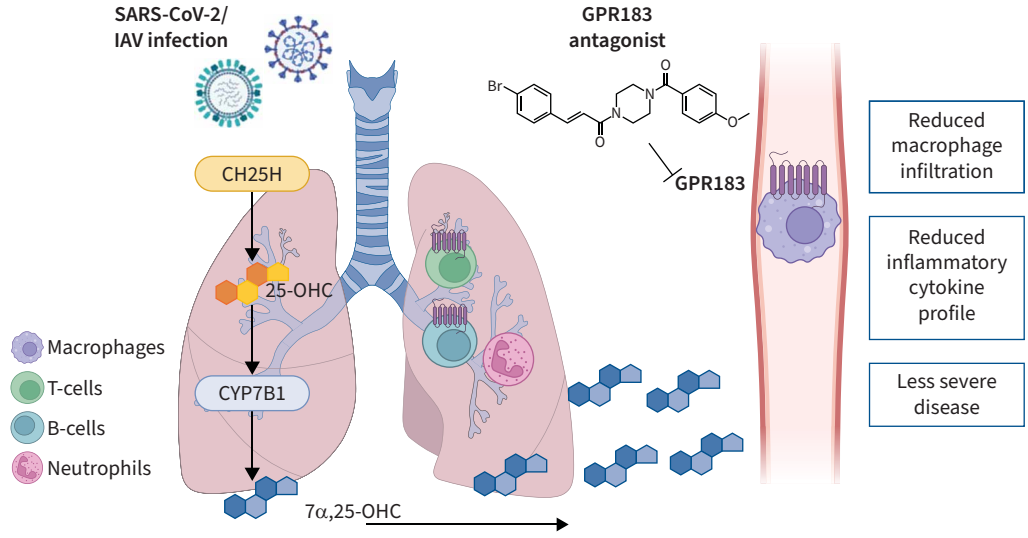

FIGURE 9 Graphical abstract of the role of GPR183 in the immune response to severe acute respiratory syndrome coronavirus 2 (SARS-CoV-2) and influenza A virus (IAV) infection. SARS-CoV-2 and IAV infection lead to the upregulation of cholesterol 25-hydroxylase (CH25H) and cytochrome P450 family 7 subfamily member B1 (CYP7B1), which results in the production of 7α,25-dihydroxycholesterol (7α,25-OHC). This oxysterol chemotactically attracts GPR183-expressing macrophages to the lungs where they produce pro-inflammatory cytokines. Pharmacological inhibition of GPR183 attenuates the infiltration of GPR183-expressing macrophages, leading to reduced production of inflammatory cytokines without negatively affecting antiviral responses.

but *Ace2* expression was downregulated to a lesser extent in NIBR189-treated animals, which is consistent with lower viral loads.

In summary, we provide the first preclinical evidence of GPR183 as a novel host target for therapeutic intervention to reduce macrophage-mediated hyperinflammation, SARS-CoV-2 loads and COVID-19 severity.

Published in volume 61, issue 3 of the *European Respiratory Journal* on 9 March 2023; republished 24 March 2023 to change the reference cited in the final paragraph of the Results section.

Acknowledgements: We thank the Queensland Health Forensic and Scientific Services, Queensland Department of Health, for providing SARS-CoV-2 isolate. We thank Sumaira Hasnain from the Mater Research Institute - The University of Queensland for sharing antibodies used in this study. We acknowledge the technical assistance of the team that operates and maintains the Australian Galaxy service (https://usegalaxy.org.au/). We thank David Hume, Maher Gandhi and Jake Gratten from the Mater Research Institute – The University of Queensland for critical review of the manuscript.

Author contributions: Conceptualisation: C.X. Foo, S. Bartlett, M.J. Sweet, K.R. Short, M.M. Rosenkilde, K. Ronacher. Methodology: K.Y. Chew, H. Bielefeldt-Ohmann, B.J. Arachchige, B. Matthews, S. Reed. Investigation: C.X. Foo, S. Bartlett, K.Y. Chew, M.D. Ngo, H. Bielefeldt-Ohmann, B.J. Arachchige, B. Matthews, S. Reed, R. Wang, C. Smith, L. Burr, K. Bisht, S. Shatunova, J.E. Sinclair, R. Parry, Y. Yang, J-P. Lévesque, A. Khromykh. Writing (original draft): C.X. Foo, S. Bartlett, K. Ronacher. Writing (review and editing): all authors. Funding acquisition: S. Bartlett, K.R. Short, M.M. Rosenkilde, K. Ronacher.

Conflict of interest: S. Bartlett reports an early career seed grant from the Mater Foundation, supporting the present study. H. Bielefeldt-Ohmann reports consulting fees from Paradigm Biopharma, Queensland University of Technology and Colorado State University, outside the submitted work. M.J. Sweet reports grants from National Health and Medical Research Council of Australia, outside the submitted work. K. Bisht reports grants from the American Society of Hematology (ASH) Global Research Award, and Translational Research Institute-Mater Research LINC grant, Mater Foundation, outside the submitted work. Y. Yang reports grants from Mater Foundation, supporting the present study. J-P. Lévesque reports grants from National Health and Medical Research Council, and US Department of Defense; and royalties or licences from GlycoMimetics Inc., outside the submitted work. M.M. Rosenkilde reports support for the animal studies and breeding in Denmark of the mouse strain used in this study from Independent Research Fund Denmark; grants from Independent Research Fund Denmark, Novo Nordisk Foundation; donations from deceased Valter Alex Torbjørn Eichmuller (VAT Eichmuller)-2020-117043, and Kirsten and Freddy Johansens Foundation (KFJ) - 2017-112697; royalties from Antag Therapeutics and Bainan Biotech from patents made at the University of Copenhagen; travel support from Gordon Research Conference 2022; and is the co-founder of the following biotech companies: Antag Therapeutics, Bainan Biotech, Synklino, outside the submitted work. K.R. Short reports grants from National Health and Medical Research Council of Australia; and consulting fees from Sanofi, Novo Nordisk and Roche, outside the submitted work. K. Ronacher reports support for the present manuscript from Mater Foundation, Diabetes Australia, Australian Infectious Diseases Research Centre, Australian Respiratory Council; and grants from NIH R01 (5R01AI116039), outside the submitted work. All other authors have nothing to disclose.

Support statement: This study was supported by grants to K. Ronacher from the Mater Foundation, the Australian Respiratory Council, Diabetes Australia and the Australian Infectious Diseases Research Centre. S. Bartlett was supported by an early career seed grant from the Mater Foundation. The Translational Research Institute is supported by a grant from the Australian Government. The Danish Council for Independent Research I Medical Sciences supported M.M. Rosenkilde. M.J. Sweet, K.R. Short and J-P. Lévesque are supported by a National Health and Medical Research Council of Australia Investigator grant (1194406), Investigator Grant (2007919) and Senior Research Fellowship (1136130), respectively. Funding information for this article has been deposited with the Crossref Funder Registry.

References

1 Flerlage T, Boyd DF, Meliopoulos V, *et al.* Influenza virus and SARS-CoV-2: pathogenesis and host responses in the respiratory tract. *Nat Rev Microbiol* 2021; 19: 425–441.

2 Chen ST, Park MD, Del Valle DM, *et al.* Shift of lung macrophage composition is associated with COVID-19 disease severity and recovery. *bioRxiv* 2022; preprint [https://doi.org/10.1101/2022.01.11.475918].

3 Speranza E, Williamson BN, Feldmann F, *et al.* Single-cell RNA sequencing reveals SARS-CoV-2 infection dynamics in lungs of African green monkeys. *Sci Transl Med* 2021; 13: eabe8146.

4 Singh DK, Aladyeva E, Das S, *et al.* Myeloid cell interferon responses correlate with clearance of SARS-CoV-2. *Nat Commun* 2022; 13: 679.
5 Shen ZJ, Hu J, Kashi VP, *et al.* Epstein–Barr virus-induced gene 2 mediates allergen-induced leukocyte migration into airways. *Am J Respir Crit Care Med* 2017; 195: 1576–1585.
6 Jia J, Conlon TM, Sarker RS, *et al.* Cholesterol metabolism promotes B-cell positioning during immune pathogenesis of chronic obstructive pulmonary disease. *EMBO Mol Med* 2018; 10: e8349.
7 Sugiura H, Koarai A, Ichikawa T, *et al.* Increased 25-hydroxycholesterol concentrations in the lungs of patients with chronic obstructive pulmonary disease. *Respirology* 2012; 17: 533–540.
8 Bottemanne P, Paquot A, Ameraoui H, *et al.* 25-Hydroxycholesterol metabolism is altered by lung inflammation, and its local administration modulates lung inflammation in mice. *FASEB J* 2021; 35: e21514.
9 Foo CX, Bartlett S, Ronacher K. Oxysterols in the immune response to bacterial and viral infections. *Cells* 2022; 11: 201.
10 Mutemberezi V, Guillemot-Legris O, Muccioli GG. Oxysterols: from cholesterol metabolites to key mediators. *Prog Lipid Res* 2016; 64: 152–169.
11 Hannedouche S, Zhang J, Yi T, *et al.* Oxysterols direct immune cell migration *via* EBI2. *Nature* 2011; 475: 524–527.
12 Liu C, Yang XV, Wu J, *et al.* Oxysterols direct B-cell migration through EBI2. *Nature* 2011; 475: 519–523.
13 Emgard J, Kammoun H, Garcia-Cassani B, *et al.* Oxysterol sensing through the receptor GPR183 promotes the lymphoid-tissue-inducing function of innate lymphoid cells and colonic inflammation. *Immunity* 2018; 48: 120–132.
14 Bohrer AC, Castro E, Tocheny CE, *et al.* Rapid GPR183-mediated recruitment of eosinophils to the lung after *Mycobacterium tuberculosis* infection. *Immunity* 2022; 40: 111144.
15 Spann NJ, Glass CK. Sterols and oxysterols in immune cell function. *Nat Immunol* 2013; 14: 893–900.
16 Preuss I, Ludwig MG, Baumgarten B, *et al.* Transcriptional regulation and functional characterization of the oxysterol/EBI2 system in primary human macrophages. *Biochem Biophys Res Commun* 2014; 446: 663–668.
17 Gessier F, Preuss I, Yin H, *et al.* Identification and characterization of small molecule modulators of the Epstein–Barr virus-induced gene 2 (EBI2) receptor. *J Med Chem* 2014; 57: 3358–3368.
18 Ngo MD, Bartlett S, Bielefeldt-Ohmann H, *et al.* A blunted GPR183/oxysterol axis during dysglycemia results in delayed recruitment of macrophages to the lung during *M. tuberculosis* infection. *J Infect Dis* 2022; 225: 2219–2228.
19 Bartlett S, Gemiarto AT, Ngo MD, *et al.* GPR183 regulates interferons, autophagy, and bacterial growth during *Mycobacterium tuberculosis* infection and is associated with TB disease severity. *Front Immunol* 2020; 11: 601534.
20 Pereira JP, Kelly LM, Xu Y, *et al.* EBI2 mediates B cell segregation between the outer and centre follicle. *Nature* 2009; 460: 1122–1126.
21 Poczobutt JM, Gijon M, Amin J, *et al.* Eicosanoid profiling in an orthotopic model of lung cancer progression by mass spectrometry demonstrates selective production of leukotrienes by inflammatory cells of the microenvironment. *PLoS One* 2013; 8: e79633.
22 Zhou JH, Wang YN, Chang QY, *et al.* Type III interferons in viral infection and antiviral immunity. *Cell Physiol Biochem* 2018; 51: 173–185.
23 Liao M, Liu Y, Yuan J, *et al.* Single-cell landscape of bronchoalveolar immune cells in patients with COVID-19. *Nat Med* 2020; 26: 842–844.
24 Corry J, Kettenburg G, Upadhyay AA, *et al.* Infiltration of inflammatory macrophages and neutrophils and widespread pyroptosis in lung drive influenza lethality in nonhuman primates. *PLoS Pathog* 2022; 18: e1010395.
25 Zhou Z, Ren L, Zhang L, *et al.* Heightened innate immune responses in the respiratory tract of COVID-19 patients. *Cell Host Microbe* 2020; 27: 883–890.
26 Dawson TC, Beck MA, Kuziel WA, *et al.* Contrasting effects of CCR5 and CCR2 deficiency in the pulmonary inflammatory response to influenza A virus. *Am J Pathol* 2000; 156: 1951–1959.
27 Hoft SG, Sallin MA, Kauffman KD, *et al.* The rate of CD4 T cell entry into the lungs during *Mycobacterium tuberculosis* infection is determined by partial and opposing effects of multiple chemokine receptors. *Infect Immun* 2019; 87: e00491-19.
28 Gold ES, Diercks AH, Podolsky I, *et al.* 25-Hydroxycholesterol acts as an amplifier of inflammatory signaling. *Proc Natl Acad Sci USA* 2014; 111: 10666–10671.
29 Diamond MS, Kanneganti TD. Innate immunity: the first line of defense against SARS-CoV-2. *Nat Immunol* 2022; 23: 165–176.
30 Stanifer ML, Guo C, Doldan P, *et al.* Importance of type I and III interferons at respiratory and intestinal barrier surfaces. *Front Immunol* 2020; 11: 608645.
31 Galani IE, Triantafyllia V, Eleminiadou EE, *et al.* Interferon-λ mediates non-redundant front-line antiviral protection against influenza virus infection without compromising host fitness. *Immunity* 2017; 46: 875–890.

32 Lokugamage KG, Hage A, de Vries M, *et al.* Type I interferon susceptibility distinguishes SARS-CoV-2 from SARS-CoV. *bioRxiv* 2020; preprint [https://doi.org/10.1101/2020.03.07.982264].

33 Vanderheiden A, Ralfs P, Chirkova T, *et al.* Type I and type III interferons restrict SARS-CoV-2 infection of human airway epithelial cultures. *J Virol* 2020; 94: e00985-20.

34 Wang S, Li W, Hui H, *et al.* Cholesterol 25-hydroxylase inhibits SARS-CoV-2 and other coronaviruses by depleting membrane cholesterol. *EMBO J* 2020; 39: e106057.

35 Zang R, Case JB, Yutuc E, *et al.* Cholesterol 25-hydroxylase suppresses SARS-CoV-2 replication by blocking membrane fusion. *Proc Natl Acad Sci USA* 2020; 117: 32105–32113.

36 Sinha S, Cheng K, Schaffer AA, *et al. In vitro* and *in vivo* identification of clinically approved drugs that modify ACE2 expression. *Mol Syst Biol* 2020; 16: e9628.

37 Saheb Sharif-Askari N, Saheb Sharif-Askari F, Alabed M, *et al.* Effect of common medications on the expression of SARS-CoV-2 entry receptors in kidney tissue. *Clin Transl Sci* 2020; 13: 1048–1054.

38 Li J, Liao X, Zhou Y, *et al.* Association between glucocorticoids treatment and viral clearance delay in patients with COVID-19: a systematic review and meta-analysis. *BMC Infect Dis* 2021; 21: 1063.